Molecular Therapy
Nucleic Acids
Original Article

miR-7 Restores Phenotypes in Myotonic Dystrophy Muscle Cells by Repressing Hyperactivated Autophagy

Maria Sabater-Arcis,[1,2,3] Ariadna Bargiela,[1,2,3] Denis Furling,[4] and Ruben Artero[1,2,3]

[1]Translational Genomics Group, Incliva Health Research Institute, Valencia 46100, Spain; [2]Interdisciplinary Research Structure for Biotechnology and Biomedicine (ERI BIOTECMED), University of Valencia, Valencia 46100, Spain; [3]CIPF-INCLIVA Joint Unit, Valencia 46012, Spain; [4]Sorbonne Université, Inserm, Association Institut de Myologie, Centre de Recherche en Myologie, Paris 75013, France

Unstable CTG expansions in the 3' UTR of the *DMPK* gene are responsible for myotonic dystrophy type 1 (DM1) condition. Muscle dysfunction is one of the main contributors to DM1 mortality and morbidity. Pathways by which mutant *DMPK* trigger muscle defects, however, are not fully understood. We previously reported that *miR-7* was downregulated in a DM1 *Drosophila* model and in biopsies from patients. Here, using DM1 and normal muscle cells, we investigated whether *miR-7* contributes to the muscle phenotype by studying the consequences of replenishing or blocking *miR-7*, respectively. Restoration of *miR-7* with agomiR-7 was sufficient to rescue DM1 myoblast fusion defects and myotube growth. Conversely, oligonucleotide-mediated blocking of *miR-7* in normal myoblasts led to fusion and myotube growth defects. *miR-7* was found to regulate autophagy and the ubiquitin-proteasome system in human muscle cells. Thus, low levels of *miR-7* promoted both processes, and high levels of *miR-7* repressed them. Furthermore, we uncovered that the mechanism by which *miR-7* improves atrophy-related phenotypes is independent of MBNL1, thus suggesting that *miR-7* acts downstream or in parallel to MBNL1. Collectively, these results highlight an unknown function for *miR-7* in muscle dysfunction through autophagy- and atrophy-related pathways and support that restoration of *miR-7* levels is a candidate therapeutic target for counteracting muscle dysfunction in DM1.

INTRODUCTION

Myotonic dystrophy type 1 (DM1) is an autosomal-dominant neuromuscular disease with multisystemic and variable symptoms. In the course of the disease, dysfunction is observed in many organs and tissues, specifically skeletal, cardiac, and smooth muscles and the CNS.[1] These dysfunctions lead to characteristic symptoms such as cardiac conduction defects, muscle myotonia with distress, neuropsychological abnormalities, muscle weakness, and atrophy.[2] The leading cause of mortality is sudden death due to cardiac conduction problems, arrhythmias, and respiratory failure as a result of muscle wasting.

The genetic cause of the disorder is an unstable expansion of non-coding CTG repeats located within the 3′ UTR of the *DM1 protein kinase* (*DMPK*) gene. Mutant *DMPK* transcripts are retained in the nucleus and form ribonuclear foci that are a histopathological hallmark of the disease. Chief among sequestered CUG-binding proteins are the Muscleblind-like proteins (MBNL1, 2, and 3). While MBNL1 controls fetal-to-adult splicing and polyadenylation transitions in muscle and MBNL2 seems to serve a similar role in the brain,[3] MBNL3 deficit results in progressive impairment of muscle regeneration[4] and age-associated pathologies observed in DM1.[5] CUGBP Elav-like family member 1 (CELF1) regulates alternative splicing antagonistically to MBNL1. In contrast to MBNL1, CELF1 is not sequestered into ribonuclear foci but is hyper-activated and stabilized in the cell nucleus.[6]

The mechanisms underlying muscle atrophy remain largely unknown. Atrophy has been linked to increased activity and stability of glycogen synthase kinase 3 beta (GSK3β) by CELF1 overactivation.[7] Indeed, mice that underwent early inhibition of GSK3β exhibited reduced muscle atrophy.[8] Moreover, defects in alternative exon regulation of *dystrophin* (*DMD*) were linked to defects in muscle architecture and organization, which are characteristic features of dystrophic DM1 skeletal muscles.[9] Additionally, it was demonstrated that embryonic M2 isoform of pyruvate kinase (*PKM2*), a key enzyme contributing to the Warburg effect in cancer, is significantly induced in DM1 tissue and mouse models owing to aberrant splicing. Authors suggest that Pkm2 re-expression in skeletal muscle disrupts the metabolic homeostasis and may lead to energy deficits associated with muscle weakness and wasting.[10]

However, evidence suggests that other processes might be contributing to muscle wasting in DM1. Specifically, autophagy and the ubiquitin-proteasome system are two main processes that mediate the degradation of cellular components in order to recycle them and obtain energy, thus maintaining muscle homeostasis. Autophagy

Received 21 July 2019; accepted 8 November 2019;
https://doi.org/10.1016/j.omtn.2019.11.012.

Correspondence: Ariadna Bargiela, Translational Genomics Group, Interdisciplinary Research Structure for Biotechnology and Biomedicine (ERI BIOTECMED), Incliva Health Research Institute, Valencia 46100, Spain, and CIPF-INCLIVA Joint Unit, Valencia 46012, Spain
E-mail: ariadna.bargiela@uv.es

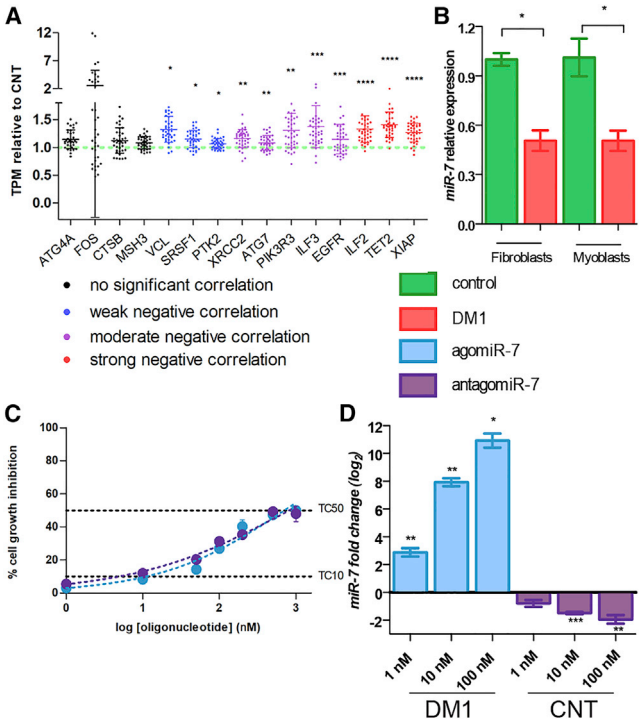

Figure 1. Involvement of *miR-7* in DM1

(A) The graph represents *miR-7* target genes that are significantly overexpressed in DM1 biopsies (according to Wang et al.[23]). Asterisks show the significance of the Pearson's correlation coefficient between ankle dorsiflexion strength and expression level of each gene. (B) Relative expression levels of *miR-7* measured by qRT-PCR (calculated using the $2^{-\Delta\Delta Ct}$ method) in human CNT (green) and DM1 (red) fibroblast and myoblast cells. (C) Cell growth inhibition assay by MTS method. Human CNT myoblasts were transfected with increasing concentrations of agomiR-7 (blue) and antagomiR-7 (purple) (n = 4). TC10 (11.15 nM for agomiR-7 and 4.92 nM for antagomiR-7) and TC50 (708.3 nM for agomiR-7 and 816.9 nM for antagomiR-7) were obtained using the least-squares non-lineal regression model. (D) Logarithmic representation on base 2 (log_2) of the qRT-PCR quantification of *miR-7* levels in human CNT (blue) and DM1 (purple) myoblasts after transfection with 1, 10, and 100 nM of agomiR-7 or antagomiR-7, respectively. Transfection of myoblasts with antagomiR-7 or agomiR-7 led to a reduction or increase of *miR-7* levels in a dose-dependent manner compared to CNT and DM1 myoblasts transfected with scramble versions of antagomiR and agomiR at the same concentration, respectively (n = 3). In (A) and (B), *U1* and *U6* snRNAs were used as reference genes (n = 3). Error bars indicate ± SEM. *p < 0.05, **p < 0.01, ***p < 0.001, ***p < 0.0001 according to Student's t test.

was demonstrated to be overactivated in DM1-derived primary myoblasts concomitantly with apoptosis, leading to loss of myotubes.[11] Consistently, autophagic markers were upregulated in mice expressing 960 CUG repeats that also exhibited marked muscle atrophy.[12] In a heat-shock-induced adult-onset DM1 *Drosophila* model, hyperactivation of autophagy and apoptosis are partly responsible for muscle atrophy, since inhibition of either pathway was sufficient to rescue muscle atrophy.[13] The defective activity of the ubiquitin-proteasome system was described in muscles of transgenic DM1 mice that displayed progressive muscle wasting and weakness due to Fbx032 and/or Murf1 overexpression.[14] Pathological activation of AMPK or TWEAK/Fn14 signaling was also reported in skeletal muscles and heart of a murine DM1 model and in tissues from DM1 patients.[15,16]

Additional studies found that the expression of several microRNAs (miRNAs) is altered in DM1 human skeletal and heart muscle and also in DM1 muscle cells.[17–19] Furthermore, misexpression was reported for 20 miRNAs in DM1 model flies. Among them, *miR-7* was under-expressed, and target transcripts had higher expression in DM1 muscle tissue, such as the autophagy-related gene *ATG4A*.[20] Interestingly, recent studies reported that *miR-7* represses autophagy through the upregulation of *mTOR* signaling and direct inhibition of some autophagy genes (*ATG7*, *ULK2*, and *ATG4A*).[21] However, the role and relevance of *miR-7* downregulation in DM1 pathogenic mechanisms still remain unknown.

Considering these previous data, here we shed light on this problem by demonstrating that depleted levels of *miR-7* trigger DM-related phenotypes through an MBNL1-independent mechanism such as increased autophagy and the ubiquitin-proteasome system, which are pathways known to contribute to muscle atrophy.[22] Importantly, replenishing of *miR-7* levels through the use of chemically modified agomiRs was sufficient to repress autophagy and muscle atrophy markers and to rescue differentiation parameters such as fusion index and myotube diameter. These results provide proof of concept that the modulation of *miR-7* levels could be a valid therapeutic approach to muscle atrophy in DM1.

RESULTS

miR-7 Targets Are Overexpressed in DM1 Muscle Biopsies and Correlate with Muscle Weakness

The first test to our hypothesis that *miR-7* levels were relevant to muscle phenotypes in DM1 was to extract expression data of direct *miR-7* target transcripts from existing datasets and to correlate their levels with functional data. To this end, we resorted to the DMseq database that includes information on ankle dorsiflexion strength from 40 DM1 patients and 10 controls.[23] From these data, the authors calculated the correlation between force and gene expression results from RNA-sequencing (RNA-seq) experiments. Based on the miRtarbase[24] and DMseq databases, we first selected all confirmed *miR-7* targets according to at least two of the following methods: 3′ UTR luciferase reporter assays, western blot, or qRT-PCR. From these genes, we selected those that were significantly overexpressed in DM1 patients, which further supported that they were under direct *miR-7* repression, and obtained a total of 11. We also included three predicted targets of *miR-7* that were studied by Fernandez-Costa et al.[20] and *ATG7*, since the binding of *miR-7* to its 3′ UTR has been demonstrated.[21] Of the 15 *miR-7* targets analyzed, 11 showed a statistically significant negative correlation (4 weak, 5 moderate, and 3 strong, according to the classification by Evans[25]) between gene expression and dorsiflexion force, that is, the higher the overexpression, the lower the force of the tibialis anterior muscle (Figure 1A; Table S1). Therefore, these results from DM1 tibialis muscle biopsies provide critical support to the hypothesis that *miR-7* levels may impinge on muscle strength, which is intimately related to muscle atrophy and weakness.

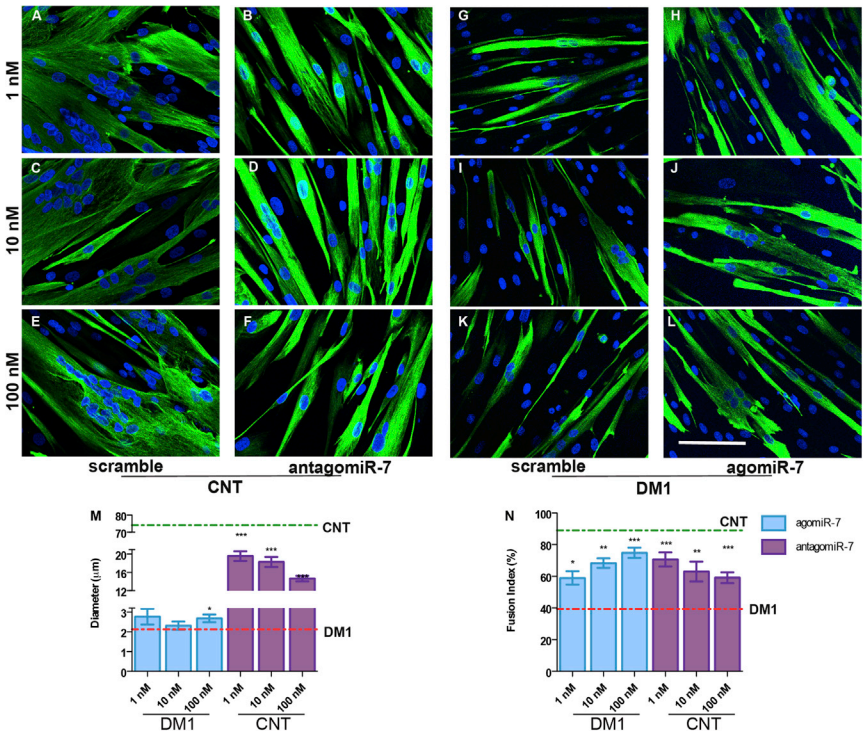

Figure 2. Raising *miR-7* Levels with agomiR Oligonucleotides Improves DM1 Myotube Defects in Fusion Capacity and Diameter

(A–L) Representative confocal images of Desmin-immunostained (green) human myoblasts transdifferentiated for 7 days after antagomiR-7 transfection into CNT cells (B, D, and F) or agomiR-7 transfection into DM1 cells (H, J, and L) and their respective scramble controls (A, C, and E for antagomiR; G, I, and K for agomiR) at 1, 10, and 100 nM. Nuclei were counterstained with DAPI (blue). Scale bar, 100 µm. (M) Quantification of myotube diameter of CNT (purple) and DM1 (blue) myoblasts treated with the indicated concentrations of antagomiR-7 and agomiR-7, respectively. Dashed lines represent the mean of the three concentrations (1, 10, 100 nM) from CNT (73.54 ± 3.77; green) or DM1 (2.24 ± 0.09; red) myoblasts transfected with scramble versions (N). Analysis of the myogenic fusion index of transdifferentiated CNT (purple) and DM1 (blue) human myoblasts transfected with antagomiR-7 or agomiR-7, respectively (n = 5–7 images in each condition; mean CNT scrambles, 89.00 ± 1.58; green dashed line, 39.37 ± 2.68; mean DM1 scrambles, red dashed line). The statistical analysis was performed comparing each concentration of agomiR-7 or antagomiR-7 to its respective scramble. Data were expressed as mean ± SEM. *$p < 0.05$, **$p < 0.01$, ***$p < 0.001$ according to Student's t test.

miR-7 Is Downregulated in 7-Day Transdifferentiated DM1 Myoblasts

Given the strong correlation between *miR-7* target dysregulation and muscle weakness in human-derived samples, we set out to establish a cell model in which we investigate the molecular basis of such a relationship. We analyzed *miR-7* levels in DM1 fibroblasts expressing 1300 CTG repeats[26] and in fibroblasts transdifferentiated into multinucleated myotubes for 7 days (Transdifferentiated myoblasts; TDM; Figure 1B). In both cases, only about half the normal levels of *miR-7* were detected in DM1 cells. We designed two chemically modified oligonucleotides as tools to investigate the potential roles of *miR-7* in DM1 muscle dysfunction: a mimic of *miR-7* (agomiR-7) and a *miR-7* blocker (antagomiR-7; Figure 1C) and assayed their toxicity profile in cells. The half-maximal inhibitory concentrations (IC_{50}) were 708.3 nM for agomiR-7 and 816.9 nM for antagomiR-7, indicating that the modified oligonucleotides were slightly toxic and they were only safe for cells at concentrations below 100 nM, at which more than 80% of cells were viable. To replenish the *miR-7* deficit, we transfected DM1 TDMs with agomiR-7 and with control (scramble) oligonucleotides at 1, 10, and 100 nM (Figure 1D, blue bars). We observed a dose-dependent increase in *miR-7* levels when compared to cells treated with the scramble at the same concentration, achieving a fold increase of over 2.100 at the highest concentration. Conversely, we decided to block *miR-7* in CNT (healthy control cells)TDMs to assess whether a lack of *miR-7* contributed to characteristic DM1 muscle phenotypes. CNT TDMs were transfected with *miR-7* antagonists and scramble controls at 1, 10, and 100 nM. After that, we quantified by qRT-PCR *miR-7* levels and observed a dose-dependent reduction of the miRNA that reached 75% of normal at 100 nM of antagomiR-7 (Figure 1D, purple bars). Note that antagomiR blocks miRNA function but not necessarily destroys it. To confirm that both the mimic and the inhibitor were effectively entering into the cells, we transfected CNT TDMs with Cy3-labeled agomiR-7 and antagomiR-7 (Figure S1). A very faint red signal was observed when cells were treated with the oligonucleotides at the lowest concentration. As expected, stronger red fluorescence was detected at 10- and 100-nM modified oligonucleotides with the number of cells being very similar in all conditions.

miR-7 Supplementation Rescues Differentiation Defects in DM1 Muscle Cells

It was previously described that DM1 myoblasts form smaller myotubes and have reduced fusion capacity under differentiation conditions.[26] We studied the contribution of *miR-7* to these phenotypes by restoring *miR-7* levels, or reducing them, in DM1 or CNT TDMs, respectively (Figure 2). After 7 days of differentiation, TDMs were stained with an antibody against Desmin, a class-III intermediate filament protein found in muscle cells that integrate the sarcolemma, Z-disk, and nuclear membrane, thus regulating sarcomere architecture and widely used as a marker of myogenic cells. DM1 TDMs had reduced diameter and fusion index compared to CNT transfected with their corresponding scramble (Figures 2G, 2I, and 2K and 2A, 2C, and 2E). Quantification of both parameters showed that DM1 TDMs had a smaller diameter than CNT, with mean values of 2.12 and 74 µm, respectively, whereas fusion index was also significantly lower (around 49.6% of normal; reference values denoted as

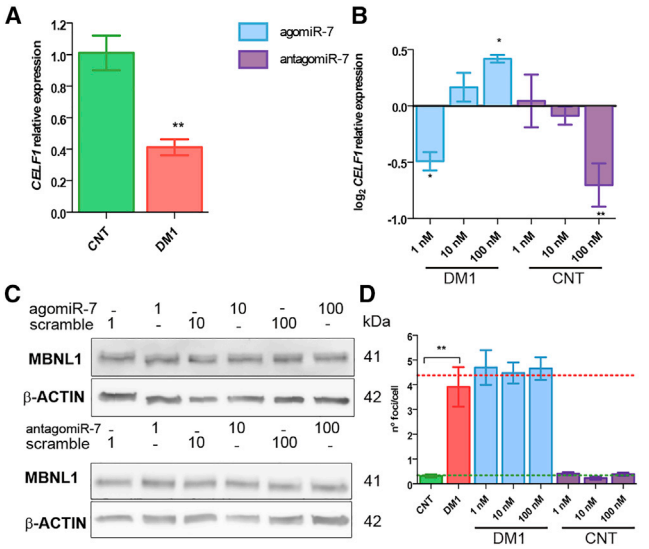

Figure 3. Modulation of *miR-7* Levels in DM1 Myoblasts Produces Changes in *CELF1* Expression, but Not in MBNL1

(A) Relative expression levels of *CELF1* measured by qRT-PCR in CNT (green) and DM1 (red) TDMs. Logarithmic representation on base 2 (log_2) of the qRT-PCR quantification of *CELF1* (B) relative expression levels in CNT (purple) and DM1 (blue) TDMs transfected with 1, 10, 100 nM of antagomiR-7 or agomiR-7. Results for each concentration of agomiR (in DM1 TDMs) or antagomiR (in control TDMs) were normalized to their corresponding scramble concentration. *GAPDH* expression levels were used as reference gene in (A) and (B) (n = 3). Data were obtained according to the $2^{-\Delta\Delta Ct}$ method. (C) Western blot of MBNL1 protein in DM1 myoblasts transfected with agomiR-7 and CNT transfected with antagomiR-7. β-ACTIN was used as endogenous control (n = 3). (D) Quantification of foci number per cell obtained from *in situ* hybridization of DM1 TDMs transfected with the indicated concentrations of *miR-7* mimic (blue bars) or CNT TDMs treated with antimiR-7 (purple bars). Dashed lines represent the mean of the three concentrations (1, 10, 100 nM) from CNT (4.398 ± 0.457; green) or DM1 (0.347 ± 0.087; red) myoblasts transfected with scramble versions. The bar graphs show mean ± SEM. *p < 0.05, **p < 0.01, ***p < 0.001 according to Student's t test.

red and green dotted lines in Figures 2M, 2N and S2). We observed that increasing the levels of *miR-7* in DM1 cells had a mild effect on the size of the myotubes, since the rescue was only statistically significant at 100 nM of agomiR. However, restoring the levels of the miRNA dramatically raised the fusion index at all three concentrations, reaching an increase of 90% when compared to the fusion index of scramble controls (Figures 2M and 2N, blue bars), which indicates an improved fusion capacity. On the contrary, a dose-dependent worsening of both parameters was observed when *miR-7* was inhibited in CNT TDMs (Figures 2M and 2N, purple bars). Taken together, these results support that while *miR-7* was necessary for both myoblast growth and fusion, only extra *miR-7* was sufficient to strongly rescue the fusion index in DM1 myoblasts. To confirm that the effect on cell fusion alterations was mediated by autophagy regulation, we inhibited or boosted this pathway by chloroquine or metformin treatment, respectively, and analyzed the fusion index (Figure S3). Results showed that this parameter was significantly improved when autophagy was blocked, and the opposite effect was observed when the pathway was induced by metformin treatment.

Restoration of *miR-7* Levels Ameliorates DM1 Phenotypes in an MBNL1-Independent Manner

To further investigate the role of *miR-7* in DM1, we analyzed the consequences of its modulation on two critical players of the disease: the CELF1 and MBNL1 genes. *CELF1* transcripts were found to respond to *miR-7* modulation so that in *miR-7*-deprived DM1 TDMs or normal TDMs transfected with antagomiR-7, *CELF1* was downregulated, whereas treatment with a *miR-7* mimic showed a dose-dependent rescue of the said defect (Figures 3A and 3B). Regulation of *CELF1* levels by *miR-7* was most likely indirect, since no significant predictions of binding were found in its 3′ UTR using the miRtarget and miRanda algorithms. In contrast, *miR-7* had no effect on MBNL1 protein levels in cells exposed to the scramble, mimic, or inhibitor oligonucleotides (Figure 3C; Figure S4A). Considering the possibility that *miR-7* could have an effect on the accumulation of mutant *DMPK* transcripts, we quantified ribonuclear foci by *in situ* hybridization. No significant differences in foci number were detected between DM1 TDMs treated with scramble and agomiR-7 (Figure 3D). We also analyzed the splicing pattern of five genes that were previously described to be regulated by MBNL1, *ATPase sarcoplasmic/endoplasmic reticulum Ca^{2+} transporting 1* (*ATP2A1*),[27] *bridging integrator 1* (*BIN1*),[28] *cardiac troponin T* (*cTNT*),[29] *DMD*,[30] and insulin receptor (*INSR*),[31] or by MBNL2, *spectrin alpha chain, non-erythrocytic 1* (*SPTAN-1*).[32] No effect was detected in any of the experimental conditions (Figure S4B). These data are consistent with unchanged MBNL1 protein levels and foci number and suggest that *miR-7* acts downstream or in parallel to MBNL1 in the DM1 pathogenesis pathway (Figure S5).

miR-7 Is a Regulatory Node for Hyperactivated Autophagy in DM1 TDMs

Deregulated autophagy was previously reported in different DM1 models, and its restoration was sufficient to recover some DM1-impaired phenotypes such as muscle mass or lifespan.[11,13,16,33] Considering this previous information and the demonstration that *miR-7* regulates *ATG4A*,[21] an autophagy regulatory gene that promotes autophagosome biogenesis,[34] we decided to measure autophagy levels in DM1 TDMs and the consequences of the modulation of *miR-7* levels on that phenotype. Autophagy was detected using LysoTracker, which is a stain with high selectivity for acidic organelles, such as digesting autophagolysosomes. CNT and DM1 TDMs were transfected with antagomiR-7 and agomiR-7, respectively, using a scramble oligonucleotide as a negative control (Figure 4). Strong green fluorescence was detected in DM1 TDMs treated with the scramble, whereas only a few green puncta were observed in CNT TDMs (compare Figures 4A, 4C, and 4E and Figures 4G, 4I, and 4K), indicating increased autophagy in DM1 cells. When *miR-7* was inhibited in CNT TDMs, a pronounced increase of the green fluorescence was detected, even at 1 nM (Figures 4A–4F). On the contrary, the transfection of DM1 TDMs with the *miR-7* mimic generated a

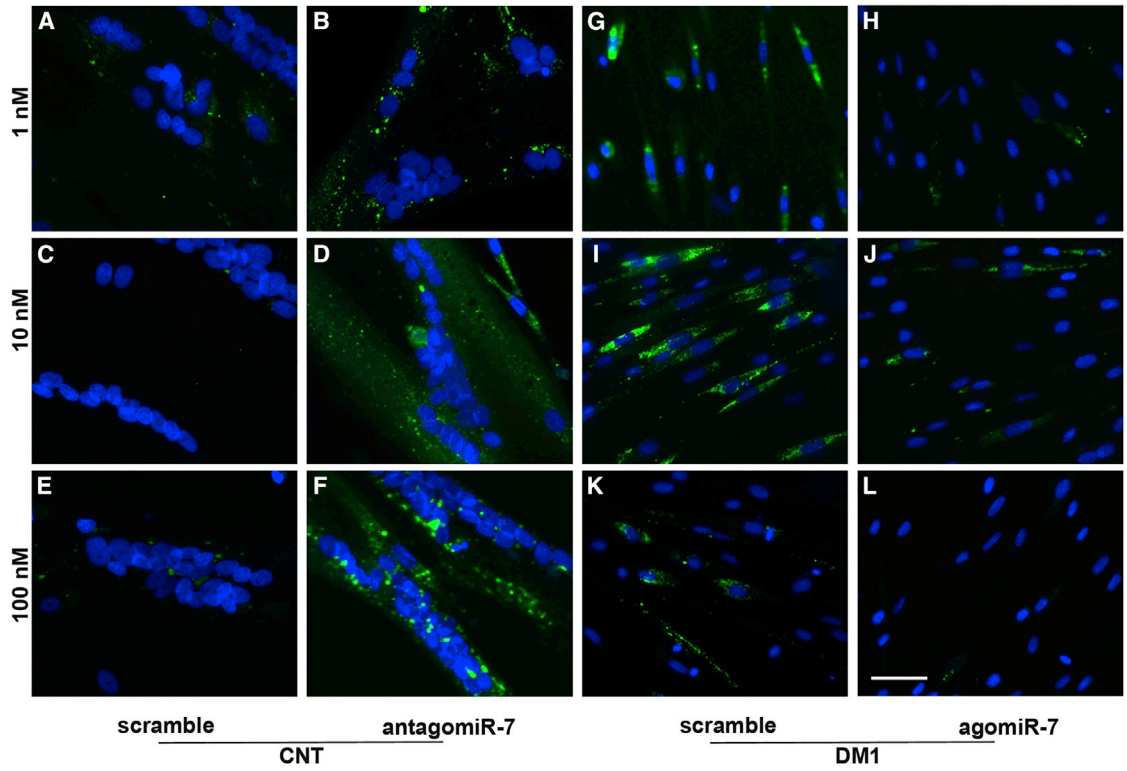

Figure 4. Restoring *miR-7* Levels Rescues Hyperactivated Autophagy in DM1 Myoblasts

(A–L) Fluorescent images of LysoTracker staining (green) in human CNT (A–F) and DM1 TDMs (G–L) treated with antagomiR-7 at 1 (B), 10 (D) and 100 nM (F) or agomiR-7 at 1 (H), 10 (J) and 100 nM (L), respectively, and their corresponding scramble controls for the antagomiR-7 1 (A), 10 (C) and 100 nM (E) or for the agomiR-7 1 (G), 10 (I) and 100 nM (K)Nuclei were counterstained with Hoechst 33342 (blue). Scale bar, 50 μm.

dramatic reduction of autophagy levels at all three tested concentrations (Figures 4G–4L).

To reinforce these observations, we analyzed by qRT-PCR the expression of six autophagy-related genes: *ATG2B*, *ATG3*, *ATG4A*, *ATG5*, *ATG7*, and *VPS34*. Importantly, we observed that all these genes were overexpressed in DM1 TDMs (Figure 5A). In contrast, in DM1 TDMs, a significant rescue of the expression levels of all the studied genes was achieved upon agomiR-7 transfection (Figures 5B–5G, blue bars). On the contrary, blocking of *miR-7* in CNT TDMs consistently enhanced expression of all five genes, yet each responded differently to varying concentrations of antimiR-7 (Figures 5B–5G, purple bars).

Autophagy activation in DM1 TDMs and response to *miR-7* was also assessed at the protein level. Amounts of ATG4A proteins were dramatically lower after the transfection of DM1 TDMs with a *miR-7* mimic, achieving values similar to those obtained in CNT cells (green dotted line, Figure 6A). Consistent results were obtained when *miR-7* was blocked in CNT TDMs, as ATG4A levels showed a potent increase of around 80%–100% compared to the same cells treated with the scramble at the same concentration. Similar results, although milder, were obtained after ATG7 quantification (Figure 6B). P62 is a scaffold protein that delivers proteins committed for lysosomal degradation to the autophagosome. Low levels of autophagic activity lead to the accumulation of P62, as the protein is degraded by autophagy itself.[35,36] Our data indicate that the transfection of DM1 TDMs with agomiR-7 at 10 and 100 nM was sufficient to totally restore P62 levels. Even at 1 nM, there was a mild but significant rescue (Figure 6C, blue bars). On the contrary, the reduction of the miRNA in CNT TDMs showed a trend to reduce P62 at the highest concentration of the *miR-7* inhibitor, thus confirming the activation of the autophagy pathway. We next evaluated levels of soluble and autophagosome-associated LC3 (LC3I and II, respectively), since the conversion of LC3I into LC3II marks the accumulation of autophagosomes in the cells[37] (Figure 6D). We observed that increasing *miR-7* levels by transfection of 100 nM agomiR achieved a reduction of autophagy in DM1 TDMs. On the contrary, by blocking the miRNA in CNT TDMs, we observed an accumulation of LC3II at all three concentrations of the inhibitor compared to the same cells treated with scramble oligonucleotide. Finally, we tested the activation of AKT and AMPK by calculating the ratio of phospho(Ser473)-AKT to AKT and phospho(Thr)172 AMPK to AMPK. This is a relevant measure, as AKT and AMPK control both protein synthesis via mTOR and protein degradation (including autophagy) via the transcription factors of the FoxO family.[38,39] We observed a

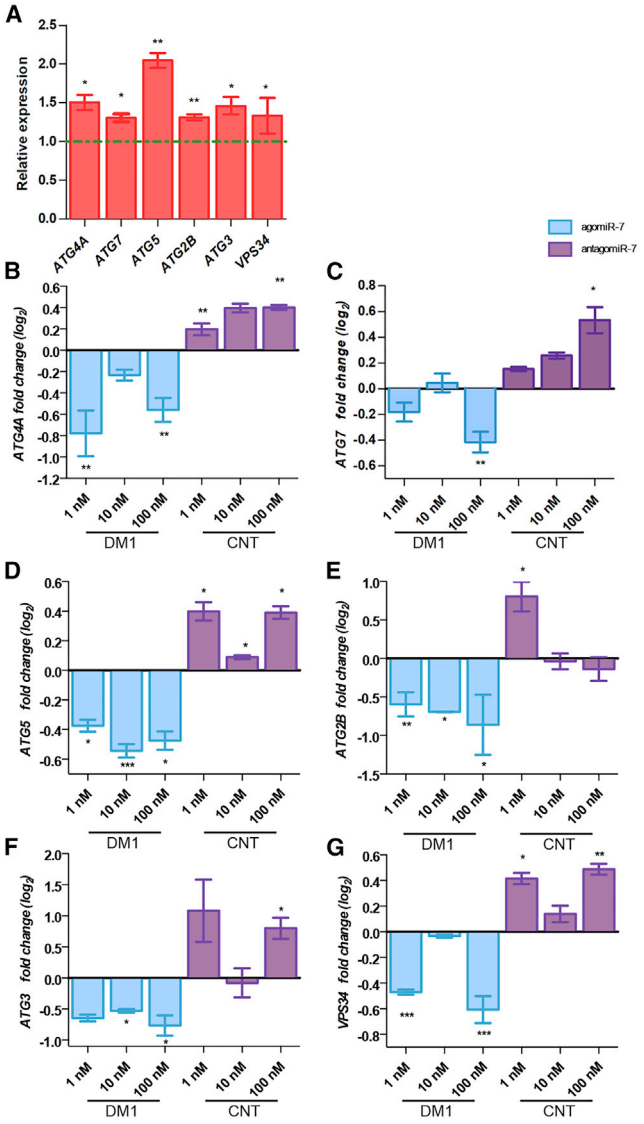

Figure 5. Impaired Expression of Autophagy-Related Genes Is Restored by Increasing *miR-7* Levels in DM1 Myoblasts

(A) Quantification of relative expression of autophagy-related genes (*ATG4A*, *ATG7*, *ATG5*, *ATG2B*, *ATG3*, and *VPS34*) in DM1 myoblasts by qRT-PCR using the $2^{-\Delta\Delta Ct}$ method. Green dashed line indicates the relative expression levels of the genes in CNT myoblasts. Logarithmic representation on base 2 (log_2) of the qRT-PCR quantification of (B) *ATG4A*, (C) *ATG7*, (D) *ATG5*, (E) *ATG2B*, (F) *ATG3*, and (G) *VPS34* in CNT (purple) and DM1 (blue) myoblasts transdifferentiated for 7 days after transfection with the indicated concentration of antagomiR-7 (in control TDMs) or agomiR-7 (in DM1 TDMs), respectively. Gene expression levels were normalized to cells transfected with antagomiR or agomiR scramble at each concentration. In all cases, *GAPDH* expression was used as reference gene (n = 3). Data were obtained using the $2^{-\Delta\Delta Ct}$ method. The bar graphs show mean ± SEM. *$p < 0.05$, **$p < 0.01$, ***$p < 0.001$ according to Student's t test.

spectacular increase in the levels of p-AKT/AKT at 100 nM agomiR-7 in DM1 TDM achieving levels slightly higher than those obtained for CNT cells transfected with scramble oligonucleotide. Conversely, CNT TDMs transfected with antagomiR-7 lowered the ratio at all three tested concentrations, except for the 10 nM condition (Figure 6E). However, no differences in AMPK ratios were observed between CNT and DM1 TDM, nor even after *miR-7* modulation (Figure S6).

To further demonstrate the relevance of *miR-7* modulation on autophagy flux, we used tandem mCherry-GFP-tagged LC3 and mCherry-GFP-tagged P62 expression vectors. The rationale behind these constructs is that GFP signal is reduced in an acidic environment, whereas mCherry is more stable. In this way, the colocalization of GFP and mCherry fluorescence indicates a cellular compartment that has not fused with an acidic organelle (autophagosome), whereas mCherry signal in the absence of GFP fluorescence corresponds to an autophagosome vesicle that has fused with a lysosome, thus becoming an autolysosome.[37] Consistent with our previous results, when we simultaneously transfected DM1 TDM cells with the vector expressing mCherry-GFP-LC3 and the scramble oligonucleotide, the signal corresponding to mCherry was much stronger than that of GFP compared to CNT TDMs, thus supporting an enhanced autophagic flux in DM1 TDM (Figures 6F and 6H). Experimental manipulation of *miR-7* levels revealed a dramatically increased autophagy flux in the CNT TDMs upon *miR-7* blocking, generating a staining pattern comparable to that of the DM1 TDMs (Figure 6G). In contrast, experimental supply of *miR-7* mimic to DM1 model cells increased GFP signal over that of mCherry, indicating alleviation of the excessive autophagic flux of DM1 cells (Figure 6I). As a control, the cells were treated with chloroquine, a compound that blocks autophagy by preventing the formation of autolysosomes (Figure 6J). In this case, the expression pattern of the reporters was very similar to that observed after the addition of agomiR-7, supporting the hypothesis that the restoration of *miR-7* levels is sufficient to normalize autophagic activity in DM1 TDMs. Similar results were obtained when cells were transfected with the construct expressing mCherry-GFP-P62 (Figure S7).

Taken together, these data demonstrate that *miR-7* plays a crucial role in the negative regulation of the autophagic pathway, as its modulation was sufficient to significantly halt (agomiR-7 in DM1 TDMs) or activate (antagomiR-7 in CNT TDMs) the process.

miR-7 Restores Expression of Genes Involved in Muscle Atrophy

Considering the impaired activation of AKT in DM1 TDMs (Figure 6E) and that AKT regulates transcription factors of the FoxO family, which subsequently regulate expression of genes involved in protein degradation, we decided to further analyze expression levels of several genes involved in these pathways. AKT1, AKT2, and AKT3 form the AKT family. In DM1 TDMs, we found that *AKT1* was downregulated and its levels could be set back to normal by transfection with 100 nM agomiR-7 (Figures 7A and 7B). Consistent with these data, silencing of AKT1 increased autophagy marker LC3II in glioma cells.[40] *AKT1* transcript levels, however, remained unchanged upon blocking of *miR-7* activity in CNT TDMs. The FoxO family in skeletal muscle is comprised of three paralogs: FoxO1, FoxO3, and FoxO4.

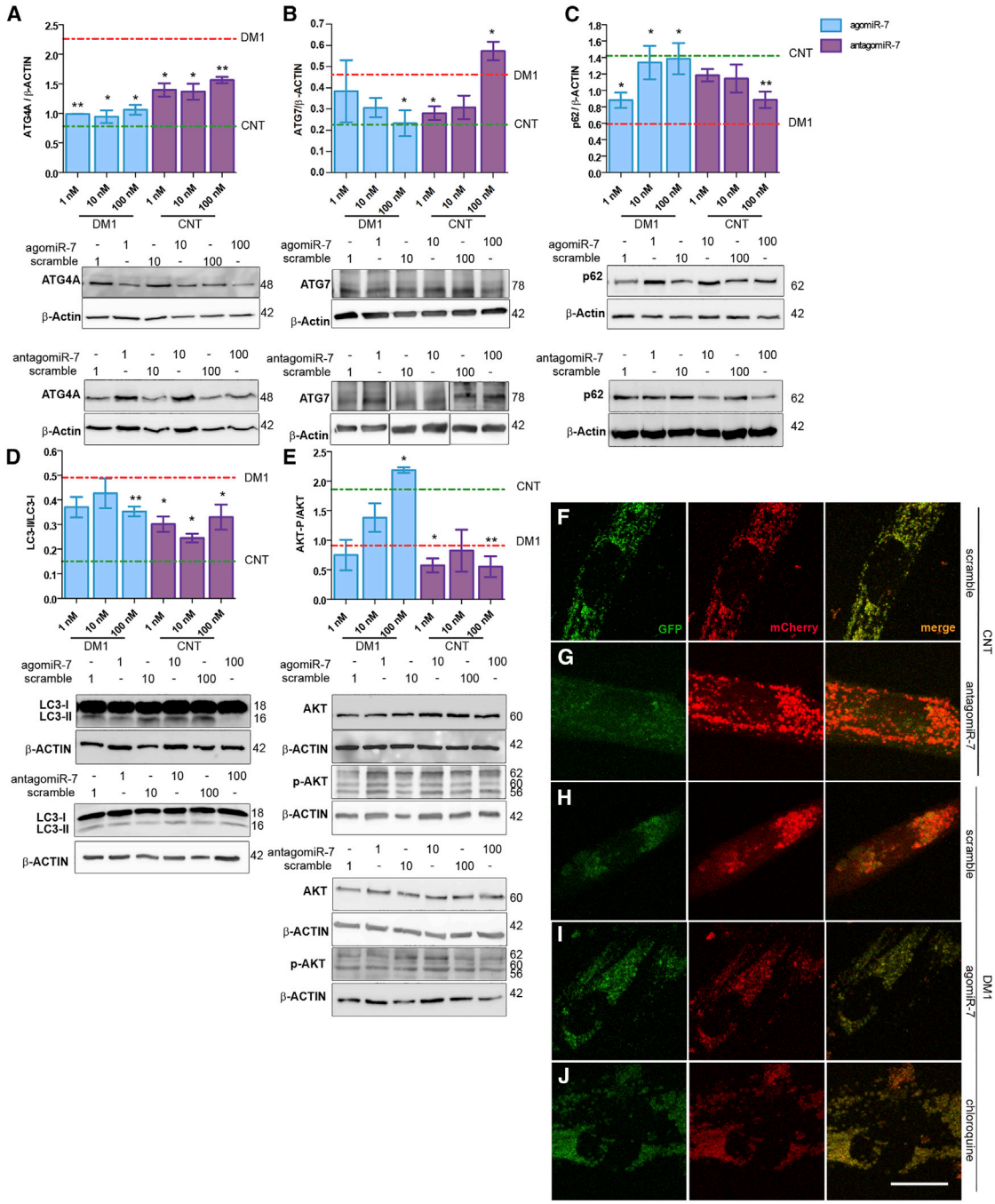

Figure 6. Positive *miR-7* Modulation Is Sufficient to Restore Autophagy-Related Protein Levels Altered in DM1 Myoblasts

Western blot analysis and representative blots of (A) ATG4A, (B) ATG7, (C) P62, (D) LC3-II/LC3-I ratio, and (E) AKT-P/AKT total protein levels in DM1 TDM (blue) treated with agomiR-7 and CNT TDM (purple) transfected with antagomiR-7 at the indicated concentrations. β-ACTIN was used as an endogenous control to normalize protein levels (n = 3). Dashed lines represent the mean of the three concentrations (1, 10, 100 nM) from CNT (0.787 ± 0.065; 0.226 ± 0.041; 1.421 ± 0.043; 0.148 ± 0.013; 1.861 ± 0.140; in A–E, respectively, green) or DM1 (2.265 ± 0.183; 0.462 ± 0.067; 0.596 ± 0.044; 0.499 ± 0.019; 0.910 ± 0.127; in A–E, respectively, red) TDMs transfected with scramble versions of the modified oligonucleotides. Representative confocal images of fluorescent LC3 puncta. CNT TDMs were cotransfected with mCherry-GFP-LC3 plasmid and 100 nM scramble oligonucleotide or antagomiR-7 (F and G). DM1 cells were cotransfected with the reporter plasmid and 100 nM scramble or agomiR-7 oligonucleotides (H and I). DM1 cells were also treated with 10 μM chloroquine for 16 h as a positive control of autophagy blockade(J). The merged images (yellow) show overlap of GFP-LC3 (green) and mCherry-LC3 (red). Scale bar represents 20 μm. Statistical analysis was performed comparing each concentration of agomiR-7 or antagomiR-7 with their respective scramble at a given concentration. The bar graphs show mean ± SEM. *p < 0.05, **p < 0.01 according to Student's t test.

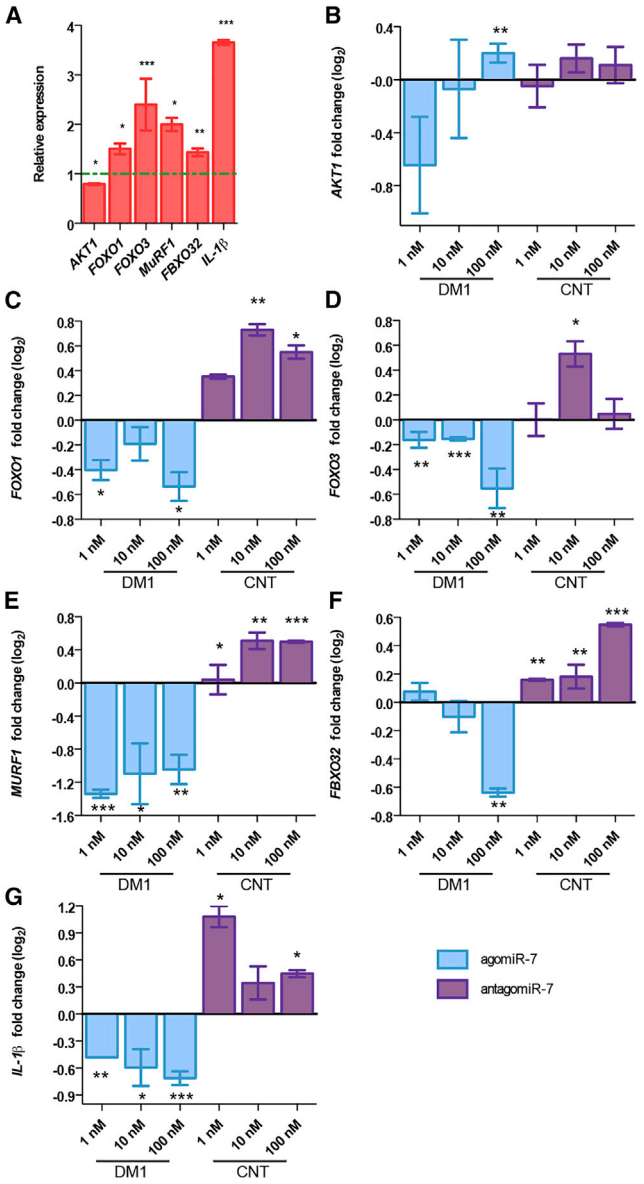

Figure 7. *AgomiR-7* Rescues Expression Levels of Genes Involved in Muscle Atrophy

(A) qRT-PCR analyses in 7-days DM1 TDMs of genes involved in signaling pathways of muscle degradation (*FOXO1*, *FOXO3*, *MuRF1*, *FBXO32*, *IL-1β*, and *AKT1*). Gene expression in DM1 TDMs was compared to the expression level of the corresponding gene in CNT TDMs (green dashed line). Logarithmic representation on base 2 (log_2) of the qRT-PCR quantification of (B) *AKT1*, (C) *FOXO1*, (D) *FOXO3*, (E) *MuRF1*, (F) *FBXO32*, and (G) *IL-1β* in CNT (purple) and DM1 (blue) TDMs treated with three concentrations (1, 10, and 100 nM) of antagomiR-7 and agomiR-7, respectively. Gene expression was normalized to cells transfected with antagomiR or agomiR scrambles at the corresponding concentration. In all cases, *GAPDH* expression was used as reference gene (n = 3). Data were obtained using the $2^{-\Delta\Delta Ct}$ method. The bar graphs show mean ± SEM. *p < 0.05, **p < 0.01, ***p < 0.001 according to Student's t test.

We quantified transcript levels of *FoxO1* and *FoxO3* and observed that they were abnormally overexpressed in DM1 TDMs, and these levels could be lowered upon transfection with a *miR-7* mimic (Figures 7A, 7C, and 7D, blue bars). We also tested the possibility of generating a DM1-like expression profile of *FoxO1* and *FoxO3* in CNT cells upon inhibition of *miR-7*, and we confirmed our hypothesis with different concentrations of antagomiR-7. *AKT*, through negative regulation of the FoxO transcription factors, downregulates the expression of *FBXO32*, *MuRF1* (involved in protein degradation), and other autophagy-related genes such as *LC3* or *BNIP3*.[41] Levels of *MuRF1* and *FBXO32* were quantified in DM1 TDMs and were found higher compared to CNT myoblasts. Both genes responded to *miR-7* manipulations as expected, and while agomiR-7 promoted lower expression, antagomiR-7 reduced it (Figures 7A, 7E, and 7F).

Skeletal muscle inflammation is one of the most common symptoms in muscle atrophy.[42] Specifically, activation of the innate immune response, as well as increased production of pro-inflammatory cytokine interleukin-1β (IL-1β) in plasma of DM1 patients were previously described.[43,44] We decided to quantify the expression levels of *IL-1β* in our cell model as an additional atrophy marker. *IL-1β* expression in DM1 TDMs was upregulated compared to CNT, supporting the notion of an immune response alteration in DM1. Surprisingly, restoration of *miR-7* levels in DM1 TDMs yielded a significant downregulation of *IL-1β* in a dose-dependent manner. In contrast, antagomiR-7 transfection in CNT increased the *IL-1β* expression at two of the three tested concentrations, thus mimicking a DM1-like phenotype (Figure 7G). Taken together, these results support the ability of *miR-7* to modulate several pathways that contribute to muscle atrophy, including ubiquitin-proteasome system.

miR-7 Modulation Affects Primary HSA^{LR} Myoblast Fusion

DM1 model mice that express 250 CTG repeat units in the context of a human skeletal actin gene (HSA^{LR})[45,46] reproduce several symptoms of the disease, such as myotonia and splicing defects, but fail to show overt muscle atrophy, according to several reports.[27,28,45] To test the hypothesis that it is lack of *miR-7* under-expression in the model that prevents atrophy, we decided to modulate levels of *miR-7* by agomiR and antagomiR administration in primary myoblasts isolated from diaphragm and gastrocnemius muscles of control (wild-type [WT]) and DM1 (HSA^{LR}) mice. First, we quantified *miR-7* levels and detected no significant differences in expression between WT and HSA^{LR} myoblasts derived from either of the analyzed muscles (Figure 8A). Of note, however, was the strong variability of *miR-7* levels among samples. Thus, we confirmed these data in diaphragm and gastrocnemius muscle samples from WT and HSA^{LR} mice, and we concluded that *miR-7* levels were normal in HSA^{LR} mice (Figure 8B). Then we treated WT myoblasts with antagomiR-7 and HSA^{LR} cells with agomiR-7, both at 50 nM. Cells were also treated with their corresponding scramble versions. *miR-7* levels dramatically increased when HSA^{LR} myoblasts were treated with agomiR-7 (Figure 8C), while blocking of *miR-7* with the antagomiR showed no effect on expression levels of the miRNA, as could be expected considering

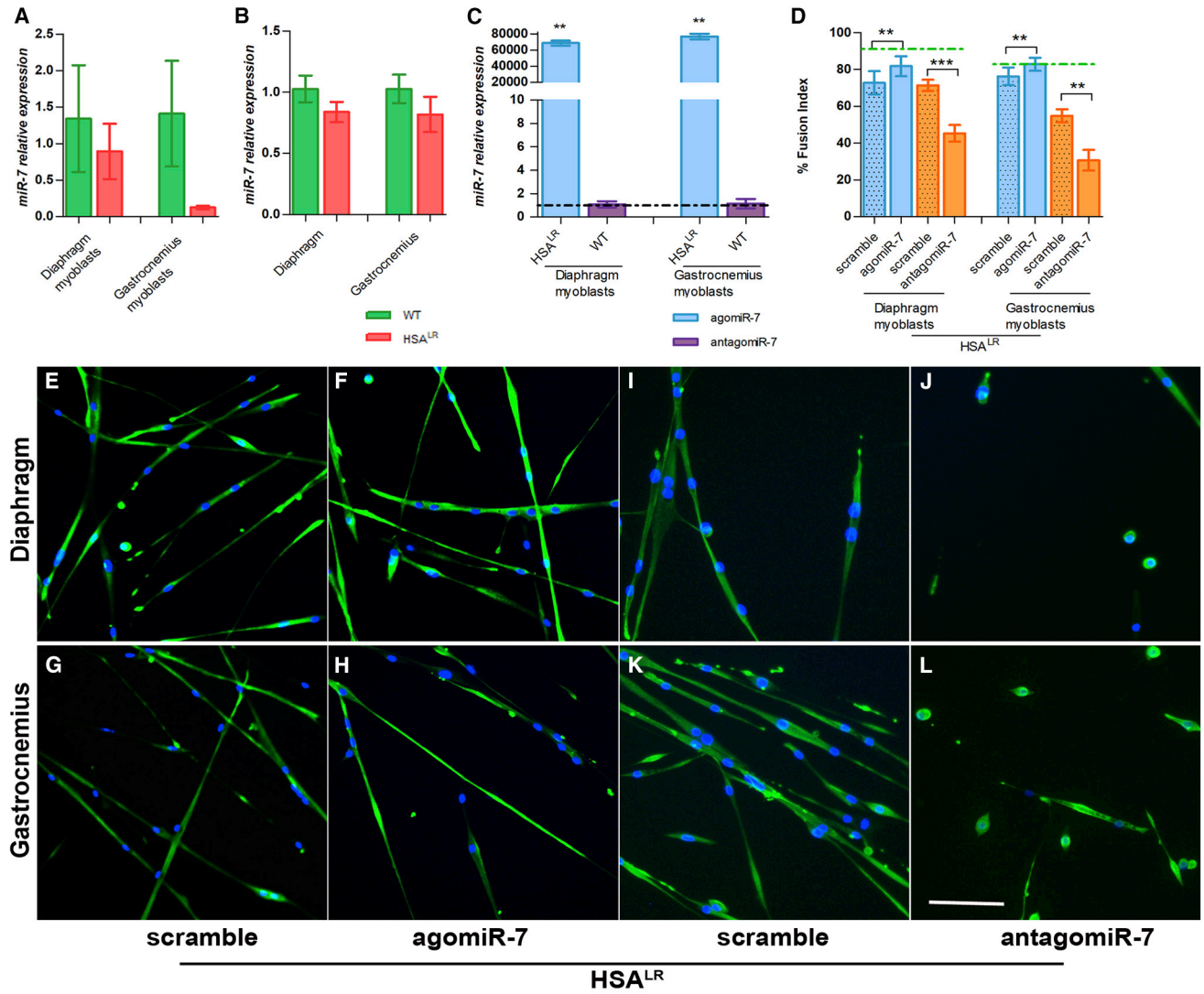

Figure 8. *miR-7* Levels Affect the Fusion Capacity of Primary Myoblasts

Quantification by qRT-PCR of relative expression of *miR-7* in (A) WT and HSA^{LR} myoblasts from the indicated tissues and in (B) gastrocnemius and diaphragm from WT and HSA^{LR} model mice. *U1* and *U6* were used as endogenous controls. Data were obtained using the $2^{-\Delta\Delta Ct}$ method (n = 3). (C) Quantification by qRT-PCR of relative expression of *miR-7* in WT and HSA^{LR} myoblasts isolated from the indicated tissues after treatment with antagomiR-7 (purple bars) or agomiR-7 (blue bars), respectively. *U1* and *U6* were used as endogenous controls. Comparisons are relative to cells treated with their corresponding scramble, indicated with the black dotted line (1.194 ± 0.663 and 1.014 ± 0.112 for HSA and WT diaphragm, respectively, and 1.053 ± 0.222 and 1.124 ± 0.366 for HSA and WT gastrocnemius, respectively). Data were obtained using the $2^{-\Delta\Delta Ct}$ method (n = 3). (D) Analysis of the myogenic fusion index of HSA^{LR} mouse myoblasts from the indicated tissues transfected with agomiR-7, antagomiR-7, or their respective scrambles (n = 7–10 images in each condition). Green dashed lines represent the mean fusion index from WT myoblasts treated with scramble versions (see Figure S8). The statistical analysis was performed comparing values from treated cells with their respective scramble. The bar graphs show mean ± SEM. *p < 0.05, **p < 0.01, ***p < 0.001 according to Student's t test. (E–L) Representative confocal images of Desmin-immunostained (green) in HSA^{LR} myoblasts from Diaphragm and Gastrocnemius treated with agomiR-7 and their scramble (F and E for Diaphragm and H and G for Gastrocnemius) or antagomiR-7 and their scramble (J and I for Diaphragm and L and K for Gastrocnemius) . Nuclei were counterstained with DAPI (blue). Scale bar, 100 μm.

the fact that the antagomiR binds to the natural miRNA blocking its activity but not necessarily promoting its degradation. The fusion index of the myoblasts was analyzed by Desmin immunostaining. We observed that this parameter was significantly reduced in gastrocnemius and diaphragm ($p = 0.0030$ and $p < 0.0001$) HSA^{LR} myoblasts compared to WT myoblasts (Figure S8). We also found that treatment with antagomiR-7 in WT myoblasts was sufficient to significantly reduce the fusion index in both myoblast lines (Figure S8). In contrast, recovery of the phenotype was detected upon replenishing *miR-7* with the agomiR in HSA^{LR} cells from diaphragm and gastrocnemius (Figures 8D–8H). To test the possibility that it is high levels of *miR-7* in HSA^{LR} myoblasts that prevent them from stronger fusion

index phenotypes, we measured this parameter after treating HSA^{LR} cells with antagomiR-7. These experiments revealed a robust reduction in the fusion index when *miR-7* activity was inhibited by the antisense oligonucleotide (Figures 8D and 8I–8L). In this case, we detected around 60% reduction in the fusion index of HSA^{LR} myoblasts treated with antagomiR-7 when compared to WT cells, similarly to values obtained in CNT and DM1 human myoblasts. Thus, like human myoblasts, primary mouse myoblasts respond to *miR-7* levels so that downregulation enhances differentiation defects and replenishment in CUG-expressing cells rescues them.

DISCUSSION

Muscle atrophy is the most debilitating symptom in DM1,[2] but the triggering molecular mechanisms are poorly understood. In the present study, we first correlated levels of *miR-7* target mRNAs with ankle dorsiflexion weakness in DM1 patients. We then used a DM1 myoblast cell model to demonstrate that *miR-7* was downregulated and the autophagic flux was impaired in these cells, which was consistent with previous reports.[11,13,16,20,33] Importantly, we restored the levels of *miR-7* in human DM1 myoblasts by transfection of a *miR-7* mimic and found that it was sufficient to drastically ameliorate myoblast fusion capacity in a dose-dependent manner, to restore normal autophagic flux, and to prevent overexpression of muscle-atrophy-related genes. Conversely, transfection of CNT cells with a miRNA inhibitor (antagomiR-7) generated DM1-like molecular phenotypes, including lower fusion potential of myoblasts, activation of the autophagy process, and increased expression of atrophy-related genes. These effects were MBNL1 independent, suggesting that *miR-7* acts downstream or in parallel of MBNL1 in this pathogenic pathway.

We analyzed the fusion index and diameter of DM1 myotubes after agomiR-7 transfection and, while we detected a mild improvement in the diameter, the rescue of DM1 myoblast fusion index was dramatic. Conversely, CNT treated with the *miR-7* inhibitor showed a significant deterioration in both parameters, which further supports a role for *miR-7* in the atrophic process. In line with these observations, normal levels of *miR-7* in HSA^{LR} cells might explain both the mild fusion defects detected and weak rescue of fusion index by agomiR-7. Indeed, a *miR-7* blocker strongly enhanced cell fusion defects. Our data suggest that *miR-7* is necessary and sufficient to sustain myoblast fusion, but, while it is required for myotube growth, additional molecular defects may remain in DM1 myotubes because replenishing of *miR-7* levels was only capable of a mild improvement of this phenotype. Importantly, independent evidence supports that fine-tuning of autophagy is critical to normal muscle differentiation. Fortini et al.[47] observed that during myogenesis, a given amount of basal autophagy is required, as a part of the metabolic reprogramming, to achieve appropriate myotube fusion. By contrast, they demonstrated that hyperactivated autophagy, by rapamycin induction, markedly inhibited myoblasts fusion. Hence, in our case, we propose that the abnormal activation of autophagy may directly contribute to the myoblast fusion defect, and thus, dampening the autophagy flux by agomiR-7 treatment explains the recovery in myoblast fusion capacity.

Notably, we disfavor the possibility that *miR-7* acts through MBNL1 regulation, as we did not observe any changes in MBNL1 protein levels, nor in several MBNL1-dependent splicing events, in DM1 and CNT muscle cells after transfection with agomiR-7 and antagomiR-7, respectively. Specifically, changes in *DMD* exon 78 regulation were monitorized. The study of this splicing event was of particular interest, as it was demonstrated to be involved in muscle atrophy and muscle weakness in DM1.[9] However, these results do not exclude a role of MBNL1 in the atrophic process, since in DM1 model flies, overexpression of *mblC* managed to rescue cross-sectional muscle area.[13] Instead, we hypothesize that *miR-7* acts downstream of MBNL1, or in parallel, in the CTG-mediated muscle disease pathways (Figure S5).

In the skeletal muscle, the ubiquitin-proteasomal system and autophagy constitute the major catabolic processes for protein breakdown. Interestingly, previous reports found a significant increase in trypsin-like proteasome activity and *Fbxo32* (*Atrogin-1*) expression in the muscles of mice expressing 45 kb of mutant human *DMPK*, thus indicating that the UPS may contribute to progressive muscle wasting and weakness.[14] Overactivation of the UPS was also confirmed in the DMSXL DM1 mouse model.[48] Consistently, our data suggest that the pathological activation of the UPS and autophagy play an important role in muscle wasting since we report increased expression of *MuRF1* and *FBXO32* in DM1 TDMs. Moreover, transcription factor FoxO3, which is induced in atrophic skeletal muscle when AKT-P levels are reduced, is known to control the transcription of *FBXO32*, *MuRF1*, and other autophagy-related genes.[38] Consequently, the upregulated expression of *FoxO1* and *FoxO3* in DM1 TDMs, and reduced AKT-P, could explain the abnormal overexpression of the atrophy-/autophagy-related genes. Importantly, transfection with the *miR-7* mimic in DM1 TDMs was enough to rescue the expression of *MuRF1*, *FBXO32*, *FoxO1*, and *FoxO3* to levels close to CNT TDMs. Moreover, analyses of AMPK phosphorylation status demonstrated no alteration in DM1 TDMs, and *miR-7* modulation did not show any effect on AMPK levels. AMPK is involved in the regulation of several metabolic pathways that regulate muscle size, such as autophagy and UPS activation or inhibition of protein synthesis via mTOR blockade.[49] However, our data suggest that this pathway remains unaltered in DM1 and that, in consequence, the activation of autophagy and UPS system are AKT dependent and that *miR-7* exerts a specific effect on the AKT signaling pathway. We also report the recovery of *IL-1*β expression by agomiR-7, showing a significant downregulation of the cytokine expression. These results provide more evidence for the beneficial effect of *miR-7* upregulation in DM1 atrophy and suggest a dual negative modulation of *miR-7* on both catabolic processes (UPS and autophagy; Figure S5). Although we cannot rule out the possibility of a direct inhibition of *miR-7* on atrophy-related genes, as described in the case of autophagy,[21] only marginal predictions were found between *miR-7* and these genes (data not shown). Considering the

crosstalk between autophagy and UPS,[38] it is possible that *miR-7* directly inhibits autophagic flux and, thus, autophagy restoration prevents UPS activation (*MURF1* and *FBXO32*). Another possibility is that the *miR-7* effect is upstream of *MuRF1* and *FBXO32*, since these genes are downstream of several atrophy-related pathways.[38]

In conclusion, although the mechanisms by which mutant *DMPK* transcripts trigger *miR-7* downregulation remain unclear, by modulating *miR-7* levels we discovered that this miRNA plays a crucial role in tuning the autophagy process and other atrophy-related pathways, such as the UPS, in DM1. Consequently, we propose that *miR-7* dysregulation is the cause, at least in part, of the autophagy overactivation, which is regarded as one of the most important contributors to muscle atrophy in DM1.[11,13] Furthermore, we report the implication of *miR-7* in myoblast fusion capacity both in human-derived myoblasts and primary myoblasts from DM1 model mice. Importantly, several authors have reported that young HSA^{LR} mice (6 months) do not reproduce muscle wasting and degeneration.[27,28,45] Our results suggest that lack of *miR-7* downregulation in DM1 model mice prevents muscle-wasting phenotypes observed in human myoblasts and biopsies, in which *miR-7* is clearly under-expressed.

In this work, we demonstrate that *miR-7* is strongly downregulated in DM1 cells. Our results suggest that modulation of *miR-7* levels *in vivo* in murine models of the disease improves on muscle homeostasis and serve as proof of concept in the development of a therapeutic strategy against DM1 based on *agomiR*-7-mediated restoration of *miR-7* levels as therapeutic approach for DM1 atrophy treatment. When considering *miR-7* modulation as a therapeutic option, our proposal is to re-establish *miR-7* to control levels, not to induce overexpression of the miRNA. This is relevant because *miR-7* is involved in normal brain development.[50] Additionally, several studies highlight the importance of *miR-7* expression in the developing pancreas for normal pancreatic development and function, which may be distinct from that in the mature pancreas.[51,52] Considering the adult nature of the disease, in a treatment based in *miR-7* modulation we do not expect to interfere with the development-related functions of the miRNA.

MATERIALS AND METHODS

Chemically Modified Oligonucleotides

Cy3-labeled and non-labeled hsa-miR-7 agomiR (agomiR-7), antagomiR (antagomiR-7), and their respective scramble controls were synthesized by Creative Biogene (NY, USA) according to the following sequences:

5′-UGGAAGACUAGUGAUUUUGUUGU-3′ (agomiR-7 sense strand),

5′-mA*mC*mGmUmGmAmCmAmCmGmUmUmCmGmGmAmGmA*mA*mT*mT*-3′-chol (agomiR-7 antisense strand),

5′-UUCUCCGAACGUGUCACGUTT-3′ (scramble agomiR-7 control, sense strand),

5′-mA*mC*mGmUmGmAmCmAmCmGmUmUmCmGmGmAmGmA*mA*mT*mT*-3′-chol (scramble agomiR-7 control, antisense strand),

5′-mU*mG*mGmAmAmGmAmCmUmAmGmUmGmAmUmUmUmUmGmU*mU*mG*mU*-3′ (antagomiR-7), and

5′-mC*mA*mGmUmAmCmUmUmUmUmGmUmGmU-mA*mC*mA*mA*-3′-chol (scramble antagomiR-7 control),

where m denotes 2′-O-methyl-modified phosphoramidites, * denotes phosphorothioate linkages, and "chol" denotes cholesterol groups. Cy3-labeled oligonucleotides were used to visualize the distribution of the compounds in cells.

Transgenic Mice

Homozygous transgenic HSA^{LR} (line 20 b) mice were provided by Prof. C. Thornton[45] (University of Rochester Medical Center, Rochester, NY, USA) and mice with the same genetic background (Friend Virus B; FVB) were used as controls and obtained from The Jackson Laboratory. Gastrocnemius and diaphragm muscles were isolated from control mice (FVB) and DM1 model mice (HSA^{LR}) expressing 250 CUG repeats. Tissues were divided in two parts. One part was snap-frozen for RNA extraction, and the other part was used to isolate mouse primary myoblasts, as described previously.[45]

Cell Culture and Transfection Conditions

A cell model of the disease[26]consisted of normal (CNT) and DM1 (1300 CTG repeats) immortalized (hTERT) skin fibroblasts conditionally expressing MyoD. Fibroblasts were grown in DMEM with 4.5 g/L of glucose, 1% of penicillin and streptomycin (P/S), and 10% fetal bovine serum (FBS) (Gibco-BRL, Grand Island, NY, USA) Fibroblasts were transdifferentiated into myoblasts by inducing the expression of MyoD.[20] Cells were plated in muscle differentiation medium (MDM) made of DMEM 4.5 g/L glucose with 1% P/S, 2% horse serum, 1% apo-transferrin (10 mg/mL), 0.1% insulin (10 mg/mL), and 0.02% doxycycline (10 mg/mL). In all cases, the cells were grown at 37°C in a humidified atmosphere containing 5% CO_2.

Fibroblasts were transfected with agomiR-7 and antagomiR-7 using X-tremeGENE HP (Roche Life Sciences; Indianapolis, IN, USA) to final concentrations ranging from 1 to 100 nM. After 4 h, transfection reagent was replaced by MDM. Fibroblasts were in MDM for 7 days, and the medium was replaced thrice.

Myoblasts from gastrocnemius, quadriceps, and diaphragm of FVB control mice and DM1 model mice, HSA^{LR}, expressing 250 CUG repeats, were isolated as previously described.[53] Myoblasts were grown F-10/DMEM medium containing 50% Ham's F-10 medium (Gibco) and 50% DMEM (4.5% glucose and L-glutamine, Gibco), 1% P/S (Gibco), and 20% FBS (Gibco). Just before use, basic fibroblast growth factor was added to the medium (10 ng/μL, Peprotech). Myoblast differentiation to myotubes was induced by replacing F-10/DMEM

medium by other containing DMEM, 5% horse serum (Gibco), and 1% P/S. Myoblasts were transfected with modified oligonucleotides using Lipofectamine RNAiMAX transfection reagent (Invitrogen) following the manufacturer's recommendations. Oligonucleotides were at a final concentration of 50 nM. Myoblasts were differentiated for 5 days.

Immunofluorescence Staining and Fusion Index Determination

Fibroblasts were seeded in 24-well plates with 2.5×10^4 cells/well. After transfection of agomiR-7 or antagomiR-7, cells were fixed with 4% paraformaldehyde (PFA) for 15 min at room temperature followed by three washes in PBS 1×. Cells were then permeabilized with PBS-T (0.3% X-Triton in PBS), blocked (PBS-T, 0.5% BSA, 1% donkey serum) for 30 min at RT, and incubated with mouse anti-Desmin (1:50, Abcam; Cambridge, MA, USA) overnight at 4°C. After three washes with PBS-T, cells were incubated for 1 h with biotin-conjugated anti-mouse-immunoglobulin G (IgG) (1:200, Sigma-Aldrich). Signal was amplified with an Elite ABC kit (VECTASTAIN Vector Laboratories; Burlingame, CA, USA) for 30 min at RT, followed by PBS-T washes and incubation with streptavidin-fluorescein isothiocyanate (FITC) (1:200, Vector) for 45 min. Samples were counterstain mounted with VECTASHIELD mounting medium containing DAPI (Vector Laboratories) to detect the nuclei. Images were taken in a confocal microscope (FV1000, Olympus Life Science Europe; Hamburg, Germany) using a 200× magnification. In the case of chloroquine and metformin, fibroblasts were transdifferentiated for 7 days. The last 48 h, cells were treated with 10 μM chloroquine or 30 mM Metformin (Sigma-Aldrich).

The fusion index was defined as the percentage of nuclei within myotubes (>2 myonuclei) regarding the total number of nuclei in each condition. The average number of total nuclei per myotube was determined by counting over 250 nuclei from randomly chosen Desmin-positive cells (5–7 micrographs). Myotube diameters were measured at five points along the entire tube. A total of 50 myotubes were examined for each experimental condition. Three independent transfection experiments were carried out. Quantification was performed using ImageJ software (NIH).

Foci Detection

Fibroblasts were seeded into 96-well plates (1.0×10^4 cells per well). After agomiR-7 or antagomiR-7 treatment, cells were fixed in 4% PFA for 10 min at room temperature followed by washes in 1× PBS. Fixed cells were incubated in pre-hybridization buffer (2× saline sodium citrate [SSC], 30% deionized formamide) for 10 min at room temperature and hybridized with Cy3-(CAG)7-Cy3-labeled probe diluted 1:500 in hybridization buffer (40% formamide, 2× SSC, 0.2% BSA, 10% dextran sulfate, 2 mM ribonucleoside-vanadyl complex, 10% tRNA [10 mg/mL], and 10% herring sperm) for 2 h at 37°C. After hybridization, cells were washed twice with pre-hybridization buffer for 15 min at 45°C, twice with 0.5× SSC for 5 min at 37°C, and once with 1× PBS for 15 min at room temperature. Cells were then incubated with Hoechst 33342 (5 mg/mL) diluted 1:2,000 in 1× PBS for 20 min at room temperature and mounted with 20% Mowiol. Images were taken and analyzed using an IN cell analyzer 2200 imaging system.

LysoTracker Staining

2.5×10^4 cells were seeded in a 24-well plate. After treatment with oligonucleotides, cells were incubated for 30 min at 37°C with 100 nM LysoTracker Green DND-26 (Invitrogen, Life Technologies, Grand Island, NY) and 5 μg/mL Hoechst 33342 (Sigma-Aldrich). Then, cells were washed twice with warmed 1× PBS and mounted using fluorescence-mounting medium (Dako; Glostrup, Denmark). Images were immediately taken on a DM4000 Leica fluorescence microscope (Leica; Wetzlar, Germany) at 400× magnification.

Toxicity Assay

CNT cells were aliquoted in 96-well plates with 1.0×10^5 cells per well. After 24 h, cells were transfected with different agomiR-7 and antagomiR-7 concentrations (from 1 nM to 1 μM) and were transdifferentiated into myoblasts for 7 days. To measure cell viability, 20 μl of MTS/PMS ([3-(4,5-dimethylthiazol-2-yl)-5-(3-carboxymethoxyphenyl)-2-(4-sulfophenyl)-2H-tetrazolium, inner salt and phenazine methosulfate respectively) was added to each well, that contains 100 μl of medium, and was incubated for 2 h at 37°C in a humidified chamber with 5% CO_2. The conversion of MTS into soluble formazan (accomplished by dehydrogenase enzymes from metabolically active cells) was measured by absorbance at 490 nm (CellTiter 96 aqueous non-radioactive cell proliferation assay, Promega; Madison, WI, USA). Absorbance was measured using an Infinite 200 PRO plate reader (Tecan Life Sciences; Männedorf, Switzerland). Data were transformed to percentage of survival relative to cells not exposed to oligonucleotides, which was considered 100% viability.

RNA Extraction, Semiquantitative PCR, and Real-Time PCR

For each biological replicate, total RNA from 1×10^6 cells was extracted using the miRNeasy mini kit (QIAGEN; Hilden, Germany) according to the manufacturer's instructions. One microgram of RNA was digested with DNase I (Invitrogen) and reverse-transcribed with SuperScript II (Invitrogen) using random hexanucleotides. To analyze alternative splicing events, 20 ng of cDNA was used in a standard PCR reaction with GoTaq polymerase (Promega). Specific primers were used to analyze the alternative splicing of *SPTAN1*, *BIN1*, *ATP2A1*, *INSR*, *DMD*, *cTNT*, and *DLG1* in CNT and DM1 muscle cells (Table S2). qRT-PCR was performed using 2 ng of cDNA template with 5× HOT FIREPol EvaGreen qPCR mix plus (ROX) (Solis BioDyne) and QuantiFast probe PCR kit reagent (QIAGEN; Vedbaek, Denmark) and specific primers and probes (Table S3). In all cases, *GAPDH* was detected as endogenous control using 0.2 ng of cDNA. miRNA expression in cells was quantified using specific miRCURY locked nucleic acid miRNA PCR primers (Exiqon) according to the manufacturer's instructions. Relative gene expression was normalized to *U1* or *U6* small nuclear RNA (snRNA). qRT-PCRs were carried out in a Step One Plus real-time PCR system (Applied Biosystems; Foster City CA, USA). Three biological replicates and three technical replicates per biological sample were performed. Relative expression to endogenous gene and the

control group were obtained by the $2^{-\Delta\Delta Ct}$ method. Pairs of samples were compared using a two-tailed Student's t test ($\alpha < 0.05$), applying Welch's correction when necessary.

Western Blotting

For total protein extraction, 1×10^6 cells were sonicated in radioimmunoprecipitation assay (RIPA) buffer (150 mM NaCl, 1.0% IGEPAL (octylphenoxypolyethoxyethanol), 0.5% sodium deoxycholate, 0.1% SDS, 50 mM Tris-HCl [pH 8.0]) plus protease and phosphatase inhibitor cocktails (Roche Applied Science). Total protein concentration was measured at 562 nm using a BCA protein assay kit (Thermo Scientific Pierce, Grand Island, NY, USA) and BSA as protein standard. 20 μg of protein were denatured for 5 min at 100°C, electrophoresed on 12% SDS-PAGE gels, and transferred onto 0.45 μm nitrocellulose membranes (GE Healthcare). Membranes were blocked with 5% non-fat dried milk in PBS-T (0.05% Tween 20 [pH 7.4]) for 1 h, then incubated overnight at 4°C in 5% blocking solution with primary antibodies at the appropriate dilution. Primary antibodies used for blotting were rabbit anti-ATG4A (1:1,000, Cell Signaling Technology), mouse anti-SQSTM1 (1:1,000, Abcam), rabbit anti-LC3B (1:3,000, Abcam), rabbit anti-AKT (1:1000, Cell Signaling Technology; Danvers, MA, USA), mouse anti-MBNL1 (1:200, clone MB1a, The Wolfson Centre for Inherited Neuromuscular Disease, UK), rabbit anti-AMPKα (1:1,000, Cell Signaling Technology), rabbit anti-phospho-Akt (Ser473) (1:1,000, Cell Signaling Technology), rabbit anti-ATG7 (1:1,000, Cell Signaling Technology), and rabbit anti-phospho-AMPKα (Thr172) (1:1,000, Cell Signaling Technology) membranes were blocked and incubated with the primary and secondary antibodies with BSA 5% in PBS-T. Goat horseradish peroxidase (HRP)-conjugated anti-mouse-IgG (1:5,000, Sigma-Aldrich) and goat HRP-conjugated anti-rabbit-IgG (1:5,000, Sigma-Aldrich) were used as secondary antibodies and were incubated for 1 h RT. Loading control was detected with a primary mouse anti-β-Actin antibody (1 h, 1:5,000, Sigma-Aldrich) followed by HRP-conjugated anti-mouse-IgG antibody (1 h, 1:5,000, Sigma-Aldrich). Immunoreactive bands were detected using enhanced chemiluminescence (ECL) western blotting substrate (Pierce), and images were taken in an ImageQuant LAS 4000 (GE Healthcare, Pittsburgh, PA, USA). Quantification was performed using ImageJ software (NIH).

Tandem mCherry-EGFP Reporter Fluorescence Assay

3.5×10^4 immortalized fibroblasts per well were seeded in 24-well plates. The next day, cells were transfected with 100 nM of the agomiR-7 (DM1) or antagomiR-7 (CNT) and their respective scramble using Lipofectamine RNAiMAX transfection reagent (Invitrogen) following the manufacturer's recommendations. After 24 h, modified oligonucleotides in MDM were removed and replaced with fresh MDM. At day 2 of differentiation, myoblasts were transiently transfected with 1 μg of pDest-mCherry-eGFP-LC3B or pDest-mCherry-eGFP-P62 (kindly provided by Prof. Fuentes, University of Extremadura, Spain) using X-tremeGENE HP DNA transfection reagent (Roche Life Science) following the manufacturer's recommendations in Opti-MEM (Gibco) for 6 h. Then, medium was replaced with MDM. 72 h post-transfections, 5-day-differentiated myoblasts were visualized *in vivo* using LSM800 confocal microscope (Zeiss, Jena, Germany) at 400× magnification. In the case of chloroquine control, myoblasts were incubated with chloroquine 10 μM (chloroquine diphosphate salt solid, ≥ 98%, C6628 Sigma Aldrich) 16 h before visualizing the cells.

SUPPLEMENTAL INFORMATION

Supplemental Information can be found online at https://doi.org/10.1016/j.omtn.2019.11.012.

AUTHOR CONTRIBUTIONS

R.A. provided the conceptual framework for the study. D.F. generated TDM. R.A., A.B., M.S.-A., and D.F. conceived and designed the experiments and helped in the interpretation of results. M.S.-A. and A.B. performed the experiments and analyzed data. A.B. and M.S.-A. prepared the manuscript with input from R.A.

CONFLICTS OF INTEREST

The authors declare no competing interests.

ACKNOWLEDGMENTS

This work was funded by grants from the Ministerio de Economía y Competitividad (SAF2015-64500-R) and the Ministerio de Ciencia, Innovación y Universidades (RTI2018-094599-B-100), including funds from the European Regional Development Fund, to R.A. Part of the equipment employed in this work has been funded by Generalitat Valenciana and co-financed with ERDF funds (OP ERDF of Comunitat Valenciana 2014-2020). A.B. was supported by a postdoctoral fellowship (APOSTD2017/077), and M.S.-A. was supported by a predoctoral fellowship (ACIF/2018/071), both from the Conselleria d'Educació, Investigació, Cultura i Esport (Generalitat Valenciana). The authors also thank Sarah Overby for her insightful comments on the manuscript.

REFERENCES

1. André, L.M., Ausems, C.R.M., Wansink, D.G., and Wieringa, B. (2018). Abnormalities in Skeletal Muscle Myogenesis, Growth, and Regeneration in Myotonic Dystrophy. Front. Neurol. *9*, 368.

2. Foff, E.P., and Mahadevan, M.S. (2011). Therapeutics development in myotonic dystrophy type 1. Muscle Nerve *44*, 160–169.

3. Charizanis, K., Lee, K.Y., Batra, R., Goodwin, M., Zhang, C., Yuan, Y., Shiue, L., Cline, M., Scotti, M.M., Xia, G., et al. (2012). Muscleblind-like 2-mediated alternative splicing in the developing brain and dysregulation in myotonic dystrophy. Neuron *75*, 437–450.

4. Poulos, M.G., Batra, R., Li, M., Yuan, Y., Zhang, C., Darnell, R.B., and Swanson, M.S. (2013). Progressive impairment of muscle regeneration in muscleblind-like 3 isoform knockout mice. Hum. Mol. Genet. *22*, 3547–3558.

5. Choi, J., Dixon, D.M., Dansithong, W., Abdallah, W.F., Roos, K.P., Jordan, M.C., Trac, B., Lee, H.S., Comai, L., and Reddy, S. (2016). Muscleblind-like 3 deficit results in a spectrum of age-associated pathologies observed in myotonic dystrophy. Sci. Rep. *6*, 30999.

6. Kuyumcu-Martinez, N.M., Wang, G.S., and Cooper, T.A. (2007). Increased steady-state levels of CUGBP1 in myotonic dystrophy 1 are due to PKC-mediated hyperphosphorylation. Mol. Cell *28*, 68–78.

7. Jones, K., Wei, C., Iakova, P., Bugiardini, E., Schneider-Gold, C., Meola, G., Woodgett, J., Killian, J., Timchenko, N.A., and Timchenko, L.T. (2012). GSK3β mediates muscle pathology in myotonic dystrophy. J. Clin. Invest. *122*, 4461–4472.
8. Wei, C., Stock, L., Valanejad, L., Zalewski, Z.A., Karns, R., Puymirat, J., Nelson, D., Witte, D., Woodgett, J., Timchenko, N.A., and Timchenko, L. (2018). Correction of GSK3β at young age prevents muscle pathology in mice with myotonic dystrophy type 1. FASEB J. *32*, 2073–2085.
9. Rau, F., Lainé, J., Ramanoudjame, L., Ferry, A., Arandel, L., Delalande, O., Jollet, A., Dingli, F., Lee, K.Y., Peccate, C., et al. (2015). Abnormal splicing switch of DMD's penultimate exon compromises muscle fibre maintenance in myotonic dystrophy. Nat. Commun. *6*, 7205.
10. Gao, Z., and Cooper, T.A. (2013). Reexpression of pyruvate kinase M2 in type 1 myofibers correlates with altered glucose metabolism in myotonic dystrophy. Proc. Natl. Acad. Sci. USA *110*, 13570–13575.
11. Loro, E., Rinaldi, F., Malena, A., Masiero, E., Novelli, G., Angelini, C., Romeo, V., Sandri, M., Botta, A., and Vergani, L. (2010). Normal myogenesis and increased apoptosis in myotonic dystrophy type-1 muscle cells. Cell Death Differ. *17*, 1315–1324.
12. Morriss, G.R., Rajapakshe, K., Huang, S., Coarfa, C., and Cooper, T.A. (2018). Mechanisms of skeletal muscle wasting in a mouse model for myotonic dystrophy type 1. Hum. Mol. Genet. *27*, 2789–2804.
13. Bargiela, A., Cerro-Herreros, E., Fernandez-Costa, J.M., Vilchez, J.J., Llamusi, B., and Artero, R. (2015). Increased autophagy and apoptosis contribute to muscle atrophy in a myotonic dystrophy type 1 Drosophila model. Dis. Model. Mech. *8*, 679–690.
14. Vignaud, A., Ferry, A., Huguet, A., Baraibar, M., Trollet, C., Hyzewicz, J., Butler-Browne, G., Puymirat, J., Gourdon, G., and Furling, D. (2010). Progressive skeletal muscle weakness in transgenic mice expressing CTG expansions is associated with the activation of the ubiquitin-proteasome pathway. Neuromuscul. Disord. *20*, 319–325.
15. Yadava, R.S., Foff, E.P., Yu, Q., Gladman, J.T., Kim, Y.K., Bhatt, K.S., Thornton, C.A., Zheng, T.S., and Mahadevan, M.S. (2015). TWEAK/Fn14, a pathway and novel therapeutic target in myotonic dystrophy. Hum. Mol. Genet. *24*, 2035–2048.
16. Brockhoff, M., Rion, N., Chojnowska, K., Wiktorowicz, T., Eickhorst, C., Erne, B., Frank, S., Angelini, C., Furling, D., Rüegg, M.A., et al. (2017). Targeting deregulated AMPK/mTORC1 pathways improves muscle function in myotonic dystrophy type I. J. Clin. Invest. *127*, 549–563.
17. Perbellini, R., Greco, S., Sarra-Ferraris, G., Cardani, R., Capogrossi, M.C., Meola, G., and Martelli, F. (2011). Dysregulation and cellular mislocalization of specific miRNAs in myotonic dystrophy type 1. Neuromuscul. Disord. *21*, 81–88.
18. Gambardella, S., Rinaldi, F., Lepore, S.M., Viola, A., Loro, E., Angelini, C., Vergani, L., Novelli, G., and Botta, A. (2010). Overexpression of microRNA-206 in the skeletal muscle from myotonic dystrophy type 1 patients. J. Transl. Med. *8*, 48.
19. Rau, F., Freyermuth, F., Fugier, C., Villemin, J.P., Fischer, M.C., Jost, B., Dembele, D., Gourdon, G., Nicole, A., Duboc, D., et al. (2011). Misregulation of miR-1 processing is associated with heart defects in myotonic dystrophy. Nat. Struct. Mol. Biol. *18*, 840–845.
20. Fernandez-Costa, J.M., Garcia-Lopez, A., Zuñiga, S., Fernandez-Pedrosa, V., Felipo-Benavent, A., Mata, M., Jaka, O., Aiastui, A., Hernandez-Torres, F., Aguado, B., et al. (2013). Expanded CTG repeats trigger miRNA alterations in Drosophila that are conserved in myotonic dystrophy type 1 patients. Hum. Mol. Genet. *22*, 704–716.
21. Gu, D.N., Jiang, M.J., Mei, Z., Dai, J.J., Dai, C.Y., Fang, C., Huang, Q., and Tian, L. (2017). microRNA-7 impairs autophagy-derived pools of glucose to suppress pancreatic cancer progression. Cancer Lett. *400*, 69–78.
22. Sandri, M. (2010). Autophagy in health and disease. 3. Involvement of autophagy in muscle atrophy. Am. J. Physiol. Cell Physiol. *298*, C1291–C1297.
23. Wang, E.T., Treacy, D., Eichinger, K., Struck, A., Estabrook, J., Olafson, H., Wang, T.T., Bhatt, K., Westbrook, T., Sedehizadeh, S., et al. (2019). Transcriptome alterations in myotonic dystrophy skeletal muscle and heart. Hum. Mol. Genet. *28*, 1312–1321.
24. Hsu, S.D., Lin, F.M., Wu, W.Y., Liang, C., Huang, W.C., Chan, W.L., Tsai, W.T., Chen, G.Z., Lee, C.J., Chiu, C.M., et al. (2011). miRTarBase: a database curates experimentally validated microRNA-target interactions. Nucleic Acids Res. *39*, D163–D169.
25. Evans, J. (1996). Straightforward Statistics for the Behavioral Sciences (Brooks/Cole Publishing).
26. Arandel, L., Polay Espinoza, M., Matloka, M., Bazinet, A., De Dea Diniz, D., Naouar, N., Rau, F., Jollet, A., Edom-Vovard, F., Mamchaoui, K., et al. (2017). Immortalized human myotonic dystrophy muscle cell lines to assess therapeutic compounds. Dis. Model. Mech. *10*, 487–497.
27. Kimura, T., Nakamori, M., Lueck, J.D., Pouliquin, P., Aoike, F., Fujimura, H., Dirksen, R.T., Takahashi, M.P., Dulhunty, A.F., and Sakoda, S. (2005). Altered mRNA splicing of the skeletal muscle ryanodine receptor and sarcoplasmic/endoplasmic reticulum Ca2+-ATPase in myotonic dystrophy type 1. Hum. Mol. Genet. *14*, 2189–2200.
28. Fugier, C., Klein, A.F., Hammer, C., Vassilopoulos, S., Ivarsson, Y., Toussaint, A., Tosch, V., Vignaud, A., Ferry, A., Messaddeq, N., et al. (2011). Misregulated alternative splicing of BIN1 is associated with T tubule alterations and muscle weakness in myotonic dystrophy. Nat. Med. *17*, 720–725.
29. Philips, A.V., Timchenko, L.T., and Cooper, T.A. (1998). Disruption of splicing regulated by a CUG-binding protein in myotonic dystrophy. Science *280*, 737–741.
30. Nakamori, M., Sobczak, K., Puwanant, A., Welle, S., Eichinger, K., Pandya, S., Dekdebrun, J., Heatwole, C.R., McDermott, M.P., Chen, T., et al. (2013). Splicing biomarkers of disease severity in myotonic dystrophy. Ann. Neurol. *74*, 862–872.
31. Savkur, R.S., Philips, A.V., and Cooper, T.A. (2001). Aberrant regulation of insulin receptor alternative splicing is associated with insulin resistance in myotonic dystrophy. Nat. Genet. *29*, 40–47.
32. Childs-Disney, J.L., Stepniak-Konieczna, E., Tran, T., Yildirim, I., Park, H., Chen, C.Z., Hoskins, J., Southall, N., Marugan, J.J., Patnaik, S., et al. (2013). Induction and reversal of myotonic dystrophy type 1 pre-mRNA splicing defects by small molecules. Nat. Commun. *4*, 2044.
33. Beffy, P., Del Carratore, R., Masini, M., Furling, D., Puymirat, J., Masiello, P., and Simili, M. (2010). Altered signal transduction pathways and induction of autophagy in human myotonic dystrophy type 1 myoblasts. Int. J. Biochem. Cell Biol. *42*, 1973–1983.
34. Abreu, S., Kriegenburg, F., Gómez-Sánchez, R., Mari, M., Sánchez-Wandelmer, J., Skytte Rasmussen, M., Soares Guimarães, R., Zens, B., Schuschnig, M., Hardenberg, R., et al. (2017). Conserved Atg8 recognition sites mediate Atg4 association with autophagosomal membranes and Atg8 deconjugation. EMBO Rep. *18*, 765–780.
35. Bjørkøy, G., Lamark, T., Pankiv, S., Øvervatn, A., Brech, A., and Johansen, T. (2009). Monitoring autophagic degradation of p62/SQSTM1. Methods Enzymol. *452*, 181–197.
36. Rusten, T.E., and Stenmark, H. (2010). p62, an autophagy hero or culprit? Nat. Cell Biol. *12*, 207–209.
37. Klionsky, D.J., Abdalla, F.C., Abeliovich, H., Abraham, R.T., Acevedo-Arozena, A., Adeli, K., Agholme, L., Agnello, M., Agostinis, P., Aguirre-Ghiso, J.A., et al. (2012). Guidelines for the use and interpretation of assays for monitoring autophagy. Autophagy *8*, 445–544.
38. Bonaldo, P., and Sandri, M. (2013). Cellular and molecular mechanisms of muscle atrophy. Dis. Model. Mech. *6*, 25–39.
39. Heras-Sandoval, D., Pérez-Rojas, J.M., Hernández-Damián, J., and Pedraza-Chaverri, J. (2014). The role of PI3K/AKT/mTOR pathway in the modulation of autophagy and the clearance of protein aggregates in neurodegeneration. Cell. Signal. *26*, 2694–2701.
40. Cheng, Y., Ren, X., Zhang, Y., Patel, R., Sharma, A., Wu, H., Robertson, G.P., Yan, L., Rubin, E., and Yang, J.M. (2011). eEF-2 kinase dictates cross-talk between autophagy and apoptosis induced by Akt Inhibition, thereby modulating cytotoxicity of novel Akt inhibitor MK-2206. Cancer Res. *71*, 2654–2663.
41. Mammucari, C., Milan, G., Romanello, V., Masiero, E., Rudolf, R., Del Piccolo, P., Burden, S.J., Di Lisi, R., Sandri, C., Zhao, J., et al. (2007). FoxO3 controls autophagy in skeletal muscle in vivo. Cell Metab. *6*, 458–471.
42. Mammarella, A., Ferroni, P., Paradiso, M., Martini, F., Paoletti, V., Morino, S., Antonini, G., Gazzaniga, P.P., Musca, A., and Basili, S. (2002). Tumor necrosis factor-alpha and myocardial function in patients with myotonic dystrophy type 1. J. Neurol. Sci. *201*, 59–64.

43. Rhodes, J.D., Lott, M.C., Russell, S.L., Moulton, V., Sanderson, J., Wormstone, I.M., and Broadway, D.C. (2012). Activation of the innate immune response and interferon signalling in myotonic dystrophy type 1 and type 2 cataracts. Hum. Mol. Genet. *21*, 852–862.

44. Zhou, J., Liu, B., Liang, C., Li, Y., and Song, Y.H. (2016). Cytokine Signaling in Skeletal Muscle Wasting. Trends Endocrinol. Metab. *27*, 335–347.

45. Mankodi, A., Logigian, E., Callahan, L., McClain, C., White, R., Henderson, D., Krym, M., and Thornton, C.A. (2000). Myotonic dystrophy in transgenic mice expressing an expanded CUG repeat. Science *289*, 1769–1773.

46. Kanadia, R.N., Shin, J., Yuan, Y., Beattie, S.G., Wheeler, T.M., Thornton, C.A., and Swanson, M.S. (2006). Reversal of RNA missplicing and myotonia after muscleblind overexpression in a mouse poly(CUG) model for myotonic dystrophy. Proc. Natl. Acad. Sci. USA *103*, 11748–11753.

47. Fortini, P., Iorio, E., Dogliotti, E., and Isidoro, C. (2016). Coordinated Metabolic Changes and Modulation of Autophagy during Myogenesis. Front. Physiol. *7*, 237.

48. Huguet, A., Medja, F., Nicole, A., Vignaud, A., Guiraud-Dogan, C., Ferry, A., Decostre, V., Hogrel, J.Y., Metzger, F., Hoeflich, A., et al. (2012). Molecular, physiological, and motor performance defects in DMSXL mice carrying >1,000 CTG repeats from the human DM1 locus. PLoS Genet. *8*, e1003043.

49. Thomson, D.M. (2018). The Role of AMPK in the Regulation of Skeletal Muscle Size, Hypertrophy, and Regeneration. Int. J. Mol. Sci. *19*, E3125.

50. Chen, H., Shalom-Feuerstein, R., Riley, J., Zhang, S.D., Tucci, P., Agostini, M., Aberdam, D., Knight, R.A., Genchi, G., Nicotera, P., et al. (2010). miR-7 and miR-214 are specifically expressed during neuroblastoma differentiation, cortical development and embryonic stem cells differentiation, and control neurite outgrowth in vitro. Biochem. Biophys. Res. Commun. *394*, 921–927.

51. Joglekar, M.V., Joglekar, V.M., and Hardikar, A.A. (2009). Expression of islet-specific microRNAs during human pancreatic development. Gene Expr. Patterns *9*, 109–113.

52. Nieto, M., Hevia, P., Garcia, E., Klein, D., Alvarez-Cubela, S., Bravo-Egana, V., Rosero, S., Damaris Molano, R., Vargas, N., Ricordi, C., et al. (2012). Antisense miR-7 impairs insulin expression in developing pancreas and in cultured pancreatic buds. Cell Transplant. *21*, 1761–1774.

53. Hindi, L., McMillan, J.D., Afroze, D., Hindi, S.M., and Kumar, A. (2017). Isolation, Culturing, and Differentiation of Primary Myoblasts from Skeletal Muscle of Adult Mice. Biol. Protoc. *7*, e2248.